77th IIW Annual Assembly and International Conference on Welding and Joining 7-12 July 2024 Rhodes, Greece

Investigations of welded joint properties of 1200M steel by laser beam welding

Raghawendra Sisodia[1*], *Marcell* Gáspár[1], *Ferenc* Hareancz[2], *Gergely* Juhász[2], and *Ferenc* Tajti[2]

[1]Institute of Materials Science and Technology, Faculty of Mechanical Engineering and Informatics, University of Miskolc, Miskolc, Hungary

[2] Department of Innovative Vehicles and Materials, GAMF Faculty of Mechanical Engineering and Computer Science, John von Neumann University, Hungary

Abstract. The emergence of modern, high-strength automotive steels necessitate the development of novel welding processes for their joining. Since the weldability study of these steels is increasingly important for their intended use in the automotive sector, laser beam welding (LBW) is considered one of the most sophisticated, versatile, and evolving processes for joining very thin sheets to thicker plates using various unique types of lasers. LBW process has significant capability to weld thin sheet metal with lower linear energy resulting narrow weld, lower deformation with higher productivity as compared to arc welding processes. However, the high strength steels (HSSs) are more prone to hardening and softening so the main aim is to analyse this behaviour of the heat affected zone (HAZ) and strength characteristics of the welded joint. In this study, a disk laser has been used to evaluate the microstructure and mechanical behaviour of the DOCOL 1200M martensitic steel with a thickness of 1 mm. The butt-welded joint configuration was used with full penetration depth and optimal parameters. Microstructure and the various mechanical tests were performed to evaluate the behaviour of HAZ and weld.

1 Introduction

In recent years, there has been a huge demand for lightweight materials in the automotive industry, especially advanced high-strength steels (AHSSs) with higher strength and better formability. Since the development of several types of cars with various fuel-propelled systems (electric, battery, hydrogen, etc.), there has been a growing need for lighter bodies that combine safety, low fuel consumption, and longer mileage [1]. The overall weight reduction in the automotive body has focused on considering environmental regulations related to CO_2 emissions reduction, etc.

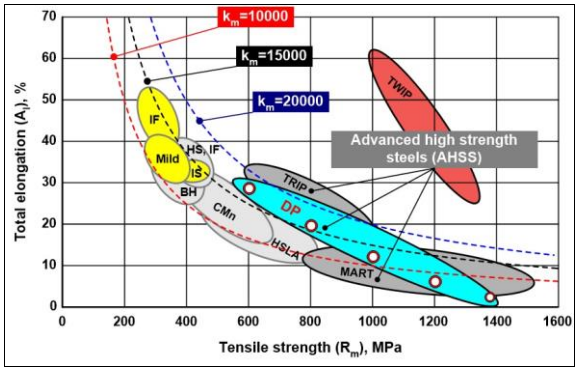

Fig. 1. Advanced high strength steels, Tensile strength vs total elongation [2, 3].

The development of AHSSs for automotive steels has been taken over the several decades in several stages like 1st generation, 2nd generation, 3rd generations steels etc.

The main HSS groups used today in the automotive industry are Complex phase (CP) steels, Martensitic (MS) steels, Ferritic-Bainitic (FB) steels, Dual Phase (DP) steels, Transformation induced plasticity (TRIP) steels, Hot-Formed (HF) and Twinning Induced Plasticity (TWIP) steels etc. In this paper, Docol 1200M steel was used for the study. The microstructure of this steel is primarily composed of martensite in a ferrite matrix. The SSAB company produces the martensitic HSSs under the brand name Docol® steel, which have an ultimate tensile strength of 900 MPa to 1700 MPa and a carbon content of 0.08% to 0.35% respectively [4, 5]. Martensitic steels have higher strength with improved ductility and can be used for more optimised design profiles, which are significantly more cost-effective than aluminium. The main application of this steel is in car body components like side impact beams, structural components etc. [4].

Fig. 1. shows the grouping of traditional and advanced high-strength steels, which typically falls into the category of thin plates. The diagram represents the tensile strength and percent elongation of different steel grades. The figure illustrates that the individual categories cannot be separated from each other strictly, only with overlaps. It can also be observed that each group is located along three characteristic curves ($R_m \times A_5 = k_m$), where R_m= ultimate tensile strength, A_5= percent elongation, and their characteristic values k_m is called the material constant [2].

The development of HSSs with higher strength also posed difficulties in the weldability, and this concern is further exacerbated by the need to maintain strength and toughness in the heat-affected zones (HAZ). Moreover, welding is the most widely used joining process in the

* Corresponding author: raghawendra.sisodia@uni-miskolc.hu

car manufacturing industry for joining different structural components. The main problem with using the typical welding processes like conventional arc or plasma arc is their higher heat input. This excessive heat causes large HAZ areas, more internal stresses and deformation, deleterious microstructures, etc., all of which ultimately affects the welded joint mechanical properties [6].

Among the various available welding processes, laser beam welding (LBW) for HSSs is the most widely and preferred welding technique. There are several types of LBW process available; however, the main types with wider applications in this field are fiber lasers, disk lasers, diode lasers etc. LBW has many peculiar characteristics compared to the arc welding process like high energy densities, low beam spot sizes, and thus high penetration depth, high welding speed, and low, precise and controlled heat input. These properties of LBW makes it exceptional in various ferrous and non - ferrous materials applications like AHSSs, titanium, Aluminium alloys etc [6, 7, 8]. Thus, the development of various laser technologies contributes to higher productivity, improved quality, reliability etc [9].

Aleksander [6] reported the most detailed, exclusive and valuable information about the continuous development of laser generators and related technologies for different types of laser radiations. This further enables the development in the field of laser materials processing like, LBW, and the application of lasers in various industrial applications, including the surface treatment of metals. Furthermore, the recent extensive research studies that focused on the Docol 1200M steel grades and various welding technological processes, including different types of LBW, are summarised. Jacek and Andrzej [7] elucidated in their study the effect of the linear energy of the LBW of the DOCOL 1200M HSS with 1.8 mm thickness on the mechanical properties of the welded joint. The welded joint strength (1240 MPa) was produced using the lowest energy (25 J/mm), which was similar to the base material (BM) strength level. The weld hardness was about 440 HV1, which was similar to BM. In the HAZ, the hardness was 360 HV1. Urban et al. [10] reported the study of fiber laser welding of Docol 1200M steel with 1 mm thickness in a lap joint arrangement. At a laser power of 300 W and a welding speed of 0.6 m/min, they reported that weld had the highest tensile-shear strength of 945 MPa, and a weld hardness of 396 HV5, which is almost the similar to the BM (400 HV5). They also mentioned that the tensile strength of the BM sample sectioned parallel to the rolling direction was 1307 MPa, and that of the sample sectioned perpendicularly to the rolling direction (RD) was 1294 MPa. The strains were 19% and 23%, respectively. These results are in good accordance with the data from manufacturer (R_m = 1289 MPa and minimal elongation of 5%) [4] . Jacek et al. [11] conducted an investigated into the structure and properties of lap joints by robotic resistance spot welding on 1.8 mm thick Docol® 1200M steel. Bożena et al. [12] in their study examining the mechanical properties of Docol 1200M welds for automotive applications, mentioned that micro-jet cooling after the MAG welding process could help maintain the initial mechanical properties of special vehicle components. Since this steel properties get affected during the welding process.

Aleksander et al. [13] studied the butt joints of double- sided zinc-coated steel sheets with a thickness of 0.8 mm by means of modern disk laser welding and investigated it effects on the microhardness, microstructure, and mechanical properties of the welded joint. They concluded that the above-mentioned properties depend on the laser welding conditions, specifically cooling rate and cooling times $t_{8/5}$ ($t_{8/5}$ cooling time represents the time in the welding thermal cycle that it will take to a welded joint to cool down from 800 to 500 °C). Eva et al. [14] stated in their study on the quality assessment of laser welding of dual phase steels that extra care is required during welding of the butt joint, which is the most frequently used joint type.

The main aim of this study is to characterize the disk laser welded martensitic 1200M steel joint using the normal disk laser welding process in order to understand the microstructural and mechanical properties of the weldments.

2 Materials and experimental procedures

The corresponding sub-sections below present the materials and experimental methods used in this study.

2.1 Base material

The base material used in this paper was uncoated, cold-rolled 1200M advanced high-strength steels in 1 mm thickness for the study of the effect of disk laser beam welding. The chemical composition and mechanical properties (according to the supplier material certificate) of the used BM are presented in Table 1 and Table 2, respectively.

Table 1. Chemical composition of base material in (%) wt.

C	Si	Mn	Cr	Ni	Mo
0.105	0.20	1.59	0.03	0.03	0.00
V	**Ti**	**Cu**	**Al**	**B**	**CEV**
0.010	0.03	0.01	0.042	0.002	0.38

Table 2. Mechanical properties of the investigated steel

Steel	Yield strength ($R_{p0.2}$), MPa	Tensile strength (R_m), MPa	Percent elongation (A_8), %	Hardness, HV0.2
1200M	1108	1289	4.5	394

Based on the data in Table 1, the calculated carbon equivalent (CEV) for the martensitic 1200M steel according to standard EN 1011-2 was 0.38.

The light optical microscopic (LOM) and scanning electron microscope (SEM) images of the investigated base material microstructure are shown in Fig. 2(a) and (b) respectively. The microstructure basically consists of martensite and some amount of ferrite.

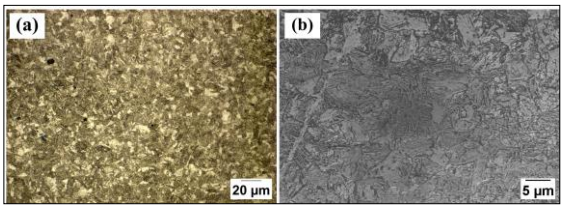

Fig. 2. Base material microstructure, 1200M steel. (a) LOM, M= 500×; (b) SEM, M= 5000×

2.2 Disk laser welding.

The laser beam welding was performed at the Department of Innovative Vehicles and Materials, John von Neumann University, Kecskemét, Hungary, by using a disk laser, TruLaser 4001 (Trumpf Laser.GmbH) with a maximum power of 4 kW and a beam parameter product (BPP) of 19.174 mm.mrad and a wavelength of 1.03 µm. According to EN 15614-11, the samples were cut into two pieces measuring 350 × 150 mm for a butt weld joint.

Before welding, the sheet joint edges and surfaces were properly cleaned with acetone to prevent distortion and ensure proper joint alignment. The sheets were clamped using a fixture. The focusing optic was an MSO100, moved by an NC machine. The TruLaser Cell 7020 laser system was used, with the laser welding head (focusing optics) equipped with a 200 mm focusing lens. A dual-core laser light cable guided the light to the processing head, with a core diameter of 100 µm and a mantle diameter of 400 µm. It operated in continuous wave (CW) mode, with a power output stability of ±1% under the rated power. The laser beam in focus had a diameter of 464 µm. During the welding experiment, the workpiece was rigidly fixed by the clamps, and the welding head moved in the welding direction.

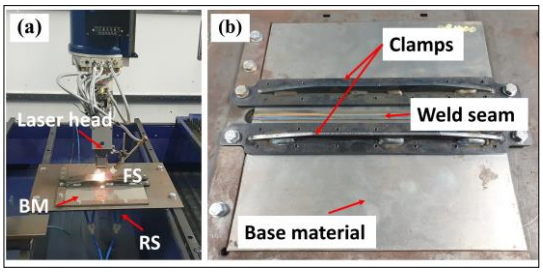

Fig. 3. LBW process; (a) Experimental set-up; and (b) Welded joint; (BM- Base material; FS- Face shielding; RS- Root shielding).

The 99.996% pure argon (Argon 4.6) gas was used for shielding on both the face side and root side of the joint at rates of 22 l/min and 10 l/min, respectively. The weld beam angle was perpendicular to the workpiece, and the nozzle-to-workpiece distance was 30 mm. The experimental setup for the disk LBW process and welded joint is shown in Fig. 3(a) and (b), respectively.

A number of welding trials were conducted to determine the optimal parameter for achieving full penetration and a sound welded joint. The optimal welding parameters used in this research are presented in Table 3. The calculated linear energy based on the optimal parameters is 74 J/mm.

Table 3. Optimum welding parameters used in evaluation.

Welding parameters	Normal welding
Laser power (Watt)	900
Welding speed (m/min)	0.73
Laser mode	Continuous
Shielding gas	Ar 4.6— 99.996%
Face side shielding gas flow rate (l/min)	22
Root side gas shielding flow rate (l/min)	10
Laser beam focussing	the focus was on the surface of sheet f = 0 mm
Wavelength (λ)	1.03

2.3 Testing methodology

To study and analyse the normal LBW process of the welded joint, microstructural and mechanical tests were performed. The metallographic, hardness, bending, tensile, and Charpy V-notch specimens were cut along the direction perpendicular to the weld seam. The microstructure of the welded joints was analysed using a light optical microscope (LOM) (Axio Observer D1m) and a scanning electron microscope (SEM) (ZEISS Sigma 300 VP). The metallographic specimens were polished with 120#, 400#, 800#, and 1500# metallographic sandpaper, and then mechanically polished to obtain a glossy mirror surface. The surface of each specimen was etched using a solution of 2% Nital to reveal the microstructure of the BM, FZ, and HAZ.

The Vickers microhardness test (Mitutoyo microhardness tester) (ISO 9015-2) was performed on the etched transverse cross sections with a load of 200 g for a 15 s dwell time. The tensile tests (ISO 4136) were performed on an MTS 322 load frame, and three-point bending test (EN 5173) was evaluated on an MTS 311 at room temperature. The instrumented Charpy V-notch impact tests were conducted using Heckert impact testing equipment equipped with a digital signal oscilloscope and a data acquisitions system.

3 Results and discussions

3.1 Microstructural test

The microstructural examination was performed using scanning electron microscopy (SEM). The weld cross section of the normal laser welded joints are shown in Fig. 4. The microstructure of the FZ and different subzones of the HAZ, i.e., fine-grained heat-affected zone (FGHAZ), intercritical heat-affected zone (ICHAZ), and subcritical heat-affected zone (SCHAZ)— for normal LB-weld are shown in Fig.4.

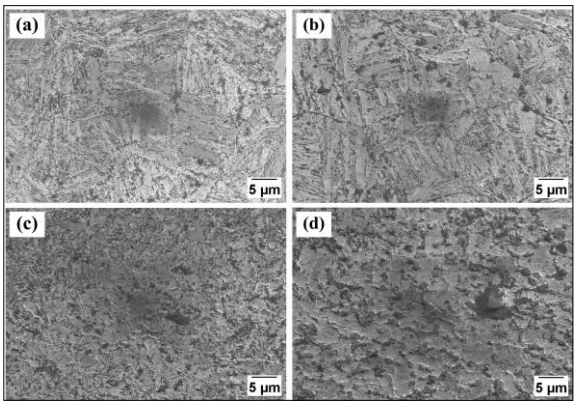

Fig. 4. Microstructure of 1200M steel in FZ and different HAZ sub-zones. (a) FZ, (b) FGHAZ, (c) ICHAZ, and (d) SCHAZ. M= 5000×

In Fig. 4(a), the FZ shows a martensitic structure with needle size. The heat-affected zone (HAZ) contains martensitic structure is more lath type, with the subcritical heat-affected zone (SCHAZ) consisting of more tempered martensite.

3.2 Microhardness test

Vickers microhardness testing was conducted on etched samples with a load of 200 g and a dwell time of 15 s. The macro photo of the microhardness mapping pattern is shown in Fig. 5. Measurements were taken across the middle of the transverse cross-section. The indentation points were adequately spaced with a distance of 0.1 mm between them.

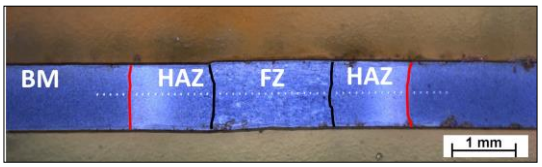

Fig. 5. Microhardness measurement macrophoto.

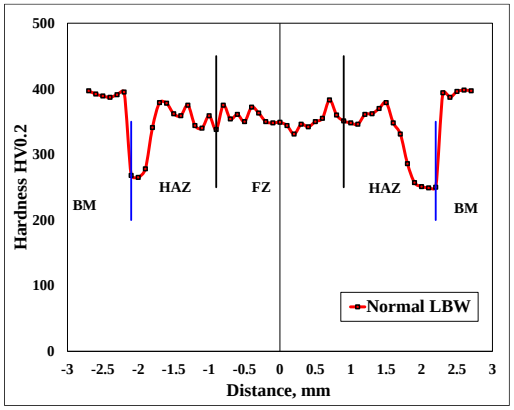

Fig. 6. Microhardness graph

Fig. 6. shows the microhardness graph of the normal LBW joint. The BM hardness was 394±4 HV0.2. The average microhardness of the FZ and HAZ was observed to be 353 HV0.2 and 320 HV0.2, respectively. The highest hardness in the HAZ was 379 HV0.2 (ICHAZ). We can observe from the results a reduction in hardness in the HAZ compared to the FZ. The width of the softened zone is greater in the HAZ (SCHAZ). To reduce the width of the softened zone, require to be use lower linear energy.

3.3 Tensile test

The transverse (perpendicular to the welding direction) tensile tests were performed according to the EN ISO 4136:2012 standard on normal LBW welded specimens. Tensile test specimens were prepared from butt-welded joints. The tensile test was carried out at room temperature using the MTS 322 tensile testing machine to determine the ultimate tensile strength of all welded specimens. The specimens were milled and etched to observe the FZ and HAZ from the welded sheets and the fracture along the welded specimens. The tensile test was performed at a rate of 0.2 mm/s. Table 4 shows the transverse tensile test results of the normal LBW welded tensile test specimens.

Table 4. Transverse tensile test results of as-welded joints specimens.

Sample No.	Tensile strength, MPa	Average tensile strength, MPa	Fracture Location
1.	1018	1023	HAZ
2.	1028		Diagonally FZ/HAZ

The results show a decrease in the tensile strength in the LB-welded joint. According to the materials certificate, the BM tensile strength was 1289 MPa. The measured average tensile strength of the welded was found to be 1023 MPa, indicating a reduction in strength of about 21%. This reduction can be attributed to the softening of the HAZ specially in the SCHAZ, and thus the rupture was observed in the HAZ. Moreover, the strength can be further improved by choosing different combinations of welding parameters while considering reducing the linear energy input. Jacek and Andrzej [7] also observed a reduction in tensile strength (from 1240 MPa to 1100 MPa) with the increase in linear energy (from 25 J/mm to 55 J/mm), and rupture occurred in the HAZ in their study with disk LBW of 1200M steel.

3.4 Bending test

The three-point bending test was performed on the MTS 311 load frame. The specimens for the tests were extracted from the transverse direction of the welded joint. Two samples each from the face side (FS) and root side (RS) of the welded joint were tested. The bending specimen dimensions were 110 mm × 24 mm. The bending test plunger diameter was 4 mm, and the distance between the centers of the fixed support rollers was 20 mm. The diameter of the fixed support roller was 10 mm. The bend test specimen and test setup are shown in Fig. 7(a) and (b), respectively. The bending test was performed at a rate of 1 mm/s, and the test results are

presented in Table 5. The static bend test results showed good plastic properties with a bending angle of 163°. However, a minor crack observed in the HAZ.

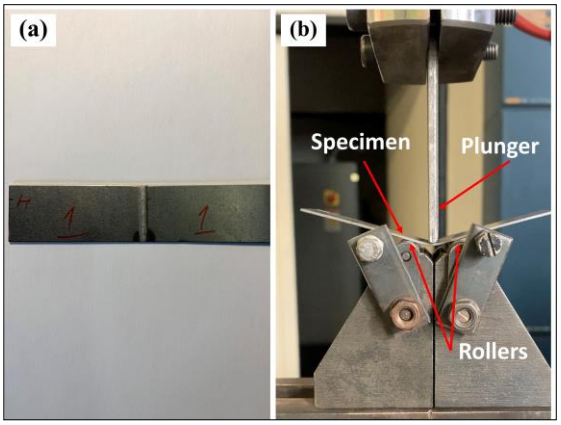

Fig. 7. Three-point bending test set-up; (a) Bending specimen, and (b) Bending test set-up.

The specimens after three-point bending tests were shown in Fig. 8.

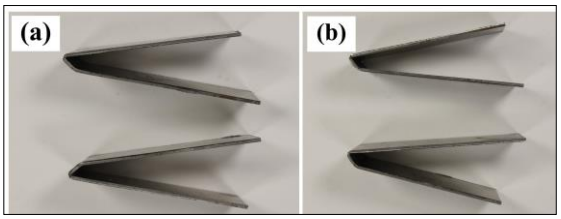

Fig. 8. Specimens after three-point bending tests: Normal LBW (a) Face side, (b) Root side.

Table 5. Bend test results.

Process	Bend side	Bend angle (°)	Result
Normal LBW	Face side	163	Crack in HAZ
	Face side	163	Crack in HAZ
	Root side	163	Crack in HAZ
	Root side	163	Crack in HAZ

3.5 Instrumented Charpy V-notch test

The instrumented Charpy V-notch test was performed on three specimens each from BM and FZ with dimensions of 10 (W) × 1 (T) × 55 (L) mm at room temperature to evaluate the impact toughness of the BM and FZ. A special designed tool was used to hold the 1 mm thickness specimens during the impact tests. Specimens were incised in the FZ.

Fig. 9. (a) and (b) represent the force-displacement graphs of the BM and FZ, respectively. In Table 6, the CVN values of the LB-welded joints from the investigated 1200M material are presented, where W_i is the crack initiation energy, W_p is the crack propagation energy and F_{max} is the maximum force.

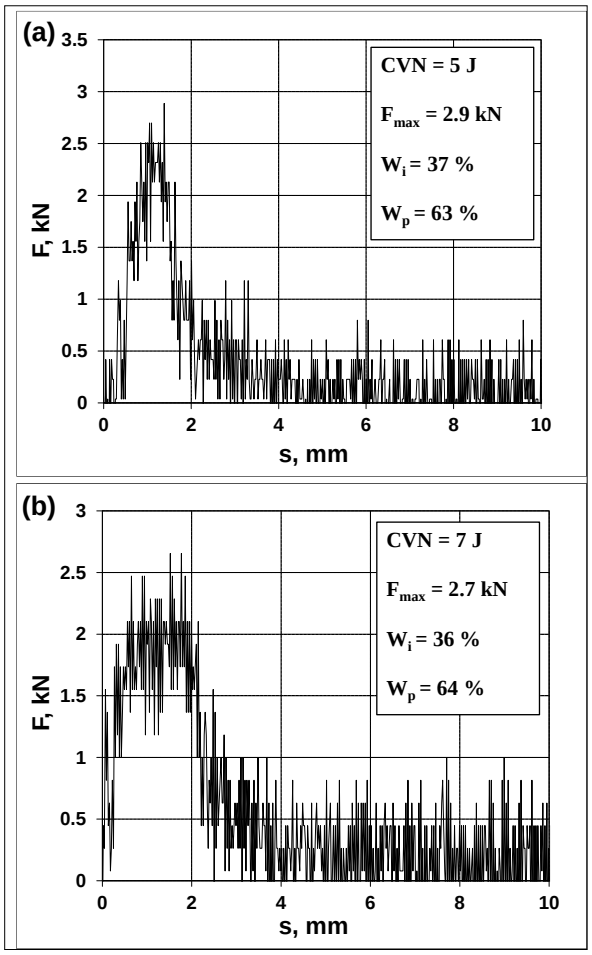

Fig. 9. Force (F)-displacement (s) graph; (a) Base material; and (b) Fusion zone.

The average impact toughness of the BM and FZ are 5 J and 7 J, respectively. The result shows an increase in toughness in the FZ compared to the BM. Considering that crack initiation occurs at the maximal force, the registered graph was divided into two parts based on the maximal force. The area under the curve until the maximum force was considered as the absorbed energy for crack initiation (W_i), while the remaining areas was for crack propagation (W_p).

Table 6. Measured values of Instrumented Charpy V-notch test.

Zone	F_{max}, kN	CVN, J	W_i, J (%)	W_p, J (%)
BM	2.9	5	1.9 (37)	3.1 (63)
	2.7	4.5	1.4 (31)	3.1 (69)
	2.3	4.5	1.5 (33)	3 (67)
FZ	2.7	7	2.5 (36)	4.5 (64)
	2.5	7	1.5 (21)	5.5 (79)
	2.9	7	1.5 (22)	5.5 (78)

The toughness of the examined material decreases with the increase of the absorbed energy ratio for the crack initiation. Thus, the FZ exhibited more absorbed

energy during the crack propagation (W_p) compared to the BM, which can also be observed from Fig. 9b, where the FZ curve is wider than that of the BM.

4 Conclusions

The study of disk laser welding of 1200M steel has been successfully conducted. The following conclusions can be drawn from the results of the microstructural and mechanical tests:

(a) The as-received BM consists of martensitic structures in a ferritic matrix, while the weld comprises martensite microstructure. HAZ consists of martensite and more tempered martensite in the SCHAZ.
(b) The average microhardness in an LBW joint was observed as 353 HV0.2 and 320 HV0.2 for the FZ and HAZ, respectively.
(c) Tensile test results showed a decrease in the strength of the weld by 21%.
(d) The bending test revealed good ductility with the applied welding parameters.
(e) Instrumented Charpy V-notch impact tests showed that the FZ of the LBW joint has higher toughness than the BM.

Based on the studies, it can be concluded that the tensile strength of the weld can reach that of the BM by using a proper combination of welding parameters, considering a lower linear energy than was used in the current study.

This paper and participation in the 77th IIW annual assembly and international conference on welding and joining, Rhodes, Greece were supported by a grant funded by the Institute of Materials Science and Technology, Faculty of Mechanical Engineering and Informatics, University of Miskolc, Miskolc-Egyetemvaros, 3515 Hungary. The participation in the IIW2024 conference was also supported by the Hungarian Welding Society (MAHEG) and the MHtE Foundation.

References

1. A. Grajcar, M. Różański, S. Stano, A. Kowalski, B. Grzegorczyk, *Adv. Mater. Sci. Eng.* **2014** 1 (2014) DOI: 10.1155/2014/658947.
2. M. Tisza, *Prod. Process. Syst.*, **6**, 79 (2013)
3. R.P.S. Sisodia, PhD Thesis, University of Miskolc (2021) DOI: https://doi.org/10.14750/ME.2021.051.
4. SSAB, Docol AHSS for the Automotive Industry, https://www.ssab.com/en/brands-and-products/docol/automotive-steel-grades/martensitic-steel/1200m, accessed: (25 May 2024)
5. S. alden Abd al al, Á. Meilinger, *Investigation of Resistance Spot Welded Joints Made on Ultra-high-Strength Steel Sheets*, in Proceedings of the International Conference on Vehicle and Automotive Engineering, VAE, 8-9 September 2022, Springer International Publishing, Cham, (2023).
6. A. Lisiecki, *Materials (Basel).*, **15**, (2022) DOI: 10.3390/ma15051765.
7. J. Górka, A. Ozgowicz, *Mater. Tehnol. / Mater. Technol.*, **52**, 2 (**2018)** DOI: 10.17222/mit.2017.077.
8. H. Zhang, M. Jiang, X. Chen, L. Wei, S. Wang, Y. Jiang, N. Jiang, Z. Wang, Z. Lei, Y. Chen, *Materials (Basel).* **15** (2022) DOI: 10.3390/ma15031095.
9. R.P.S. Sisodia, M. Gáspár, F. Hareancz, G. Juhász, *Effect of beam oscillation on weld characteristics of laser welded*, in Proc. of the 76th IIW Annual Assembly and Intl. Conf. on Welding and Joining, 16-21 July 2023, Singapore (2023)
10. U. Prijanovič, M.P. Tonkovič, U. Trdan, M. Pleterski, M. Jezeršek, D. Klobčar, *Metals (Basel).* **10**, 1 (2020) DOI: 10.3390/met10040533.
11. J. Górka, A. Ozgowicz, K. Matusek, *Weld. Technol. Rev.* **91(4)**, 33 (2019) DOI: 10.26628/wtr.v91i4.1007.
12. B. Szczucka-Lasota, T. Węgrzyn, T. Szymczak, A. Jurek, J. Piwnik, K.I. Wilczyński, *Transp. Probl.* **16(2)**, 33 (2021) DOI: 10.21307/tp-2021-021.
13. A. Lisiecki, R. Burdzik, G. Siwiec, L. Konieczny, J. Warczek, P. Folega, B. Oleksiak, *Arch. Metall. Mater.* **60**, 2913 (2015) DOI: 10.1515/amm-2015-0465.
14. E.S.V. Marques, A.B. Pereira, F.J.G. Silva, *Metals (Basel).* **12**, 1 (2022) DOI: 10.3390/met12081253.